



ACOUSTICS 2012

PIV measurements of 3-dimensional acoustic Rayleigh streaming in a square cross-section standing wave resonator

I. Reyt^a, Y. Rafat^b, L. Mongeau^b, R. Taher^b and H. Bailliet^a

^aCNRS - Université de Poitiers - ENSMA, ENSIP, 6 rue Marcel Doré, Batiment B17, BP 633, 86022 Poitiers, France

^bMcGill university, 845 Sherbrooke St. W., Montreal, Canada H3A 2T5
ida.reyt@etu.univ-poitiers.fr

Rayleigh streaming may hamper the efficiency of thermoacoustic engines by causing convective heat transfer between the stack and the heat exchangers. The characterization of the effects of Rayleigh streaming is needed to assess on quantify the efficiency of thermoacoustic devices. Streaming flows in 2D channels, between two infinite plates, and in a cylindrical duct, has been described theoretically in the literature. Among the numerous effects that make streaming in real devices differ from these ideal cases is the use of a square-section channel, which may result in complex streaming structures. In the present study, acoustic streaming in a rectangular standing wave guide was investigated experimentally. The velocity fields were measured using PIV (Particle Image Velocimetry). The measurements were performed for various measurements planes. Three-dimensional cell structures were reconstructed from the measured planar streaming velocity fields. Acoustic streaming in the near wall region was studied by zooming near the wall of the channel. Results of measurements for streaming in the square cross-section standing wave tube were compared to theoretical predictions for cylindrical wave guide.

1 Introduction

“Acoustic streaming” or “acoustic wind” refers to mean flow generated by an acoustic wave. Two types of streaming are generally considered depending on the origin of streaming driving forces. “Eckart streaming” is due to absorption in the main body of an irrotational sound beam. “Rayleigh streaming” owes its origin in boundary layer effects between a solid and a fluid. It was first modeled by Rayleigh [1] to describe Dvorak’s phenomenon associated with dust pattern in Kundt’s tube.

Thermoacoustic devices generally fail to behave as predicted by linear available model [2] and streaming is among non linear effects that are at the origin of these discrepancies. Acoustic streaming is important for the field of thermoacoustics because this nonzero time-averaged mass flow is a mechanism for convecting heat transfer that can reduce the efficiency of thermoacoustic devices. It can be present in the main resonator and also in other elements of the devices such as stack pores. A better understanding and characterization of Rayleigh streaming flows is therefore useful to assess their impact on the efficiency of thermoacoustic engines.

Rayleigh derived a solution for streaming generated by a standing wave between two infinite, widely separated plates [3]. Together with further studies by Nyborg [4] and Westervelt [5], this work yields the so-called RNW streaming theory. On the basis of this work, a number of authors worked on the theoretical description of Rayleigh streaming in order to take into account thermal effects [6, 7] and/or for channels of arbitrary width [8, 9], or to account for inertial effects [10]. All theoretical developments to date, however, have been limited to streaming generation in 2D channels, either between two infinite plates or in a cylindrical guide.

Quantitative measurements of the streaming in a standing wave guide have been performed [11, 12, 13, 14]. Experimental studies by Sharpe, Greated and collaborators (e.g. [11]) and by Thompson and Atchley (e.g. [13]) first allowed quantitative comparisons between measured and calculated streaming velocities in the core region using Particle Image Velocimetry (PIV) or Laser Doppler Velocimetry (LDV) measurements. Studies by Moreau et al. [15] allowed such comparison in a cylindrical wave-guide for the near wall region and the core, boundary layer effects being of particular importance in streaming generation. Both square [16] and cylindrical channels: [13, 15, 12] have been investigated but, because comparison with theoretical models is not systematic, the question of 3D effects linked with the use of a non-ideal channel has never been addressed.

In the present study, as a first step towards the investigation of streaming in realistic cooler configurations, the acous-

tic wind in a resonator with a square cross-section was investigated. For a horizontal waveguide, velocity fields within the horizontal plane were measured using PIV. These measurements were performed at several vertical positions so that 3D streaming cell structures could be reconstructed from the different planar streaming velocity fields. The results were compared to theoretical expectations for a cylindrical channel. Theoretical results for streaming in a cylindrical waveguide are reviewed in Section 2. Experimental procedures and measurements analysis are described in Section 3, and results are presented in Section 4.

2 Rayleigh streaming in cylindrical waveguides

In a 2D resonator with rigid walls in which a $\lambda/2$ standing wave is set up, streaming vortices consist in toroidal axially centered vortices with a periodicity of $\lambda/4$ along the waveguide axis, as shown by figure 1, with $\lambda = c/f_{ac}$ the acoustic wave length, c the velocity of sound, and f_{ac} the acoustic frequency.

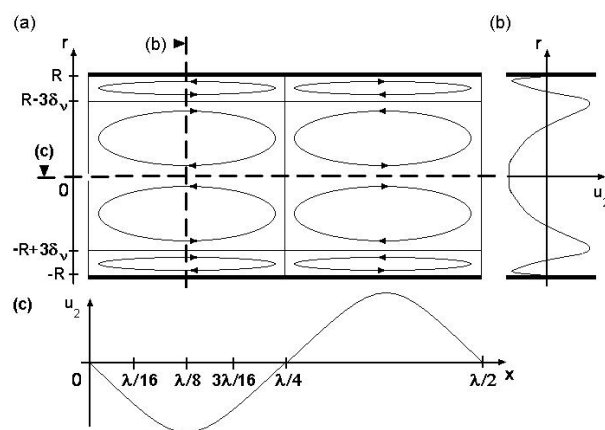


Figure 1: Schematic representation of streaming velocity field in a half wavelength resonator. a) Acoustic streaming vortices. b) Variation of axial streaming velocity with respect to the transverse coordinate r for $x = \lambda/8$. c) Variation of centerline axial streaming velocity with respect to the axial coordinate x .

Outer vortices are present in the core, that is for $R - 3\delta_v \lesssim r \lesssim -R + 3\delta_v$, with R the tube radius, $\delta_v = \sqrt{\frac{2\nu}{\omega}}$ the viscous boundary layer thickness, $\omega = 2\pi f_{ac}$ the angular frequency of acoustic oscillations, ν the kinematic viscosity of the fluid. Neighboring cells circulate in opposite directions. As stated

above, the variation of the axial streaming velocity along x is sinusoidal, with the maximum value occurring at $(2n+1)\lambda/8$, with n an integer. For the outer vortices, the variation of the axial component of streaming velocity with respect to r is parabolic. In the near wall region, the inner streaming vortices rotate in a direction opposite to that of the outer one. Note that in Figure 1, streaming is schematized for a thin guide for which $R/\delta_v \approx 10$.

In order to help visualizing the shape of streaming cells for further comparison with results of measurements in square-section guides, theoretical predictions for streaming in a cylindrical wave guide on are presented on 3D graphs. Figure 2.a shows iso-axial-velocity surfaces corresponding to streaming a velocity of $0.006m/s$. Figure 2.b shows iso-contour plots for different vertical planes. Figure 2.c shows iso-contour plots for two quadrants and for different horizontal and vertical planes. In these figures, the corresponding acoustic velocity amplitude is $3.4m/s$ and streaming was calculated using [8].

The goal of the present study was to determine the streaming structures for a square channel. Because the thermoviscous function f_v and f_k [17] or equivalently $F(\lambda)$ or $F(\lambda_T)$ [18] for a square cross-section channel are closer from the one of a circular-section channel than from the one of a parallel plate channel [18], and because Rayleigh streaming is due to boundary layer effects, we choose to compare streaming in a square-section guide to the one in a cylindrical guide.

3 Experimental procedures

3.1 Experimental apparatus

The apparatus illustrated in Figure 3 has been used to study the streaming velocity field generated by a monofrequency acoustic standing wave in air. The acoustic resonator (j) has a square cross section $4 \times 4 \text{ cm}$, and a length of $L = 98 \text{ cm}$. The walls of the resonator were 9 mm thick. A function generator (a) produced a sinusoidal excitation signal, which was fed to a 200 W acoustic driver (e) via a 200 W RMS power amplifier (d). A power analyzer (b) was connected in parallel with the acoustic driver to monitor the instantaneous true RMS voltage, current and power fed to the acoustic driver. Two high-resolution ICP pressure transducers were mounted flush near the two extremities of the resonator for measuring acoustic pressure. The PIV system was a dual-cavity, time-resolved (TR) Nd:YLF laser (g) with a maximum repetition rate of 10 kHz per cavity. A CCD-CMOS camera (f) with a frame rate of 2000 fps and a resolution of 1280×1024 pixels was used. The pixel pitch of the camera was $12 \mu\text{m}$. The camera was mounted on a traversing mechanism (i), which allowed mapping of the velocity field over the entire length of the resonator. A controller unit (c) supplied by the PIV system manufacturer was employed in order to synchronize the camera and the laser. A Laskin nozzle-seeding generator, using olive oil, produced $1 \mu\text{m}$ particles, which were used to seed the flow.

3.2 Data acquisition and analysis

Using the apparatus set-up described above, velocity fields within the horizontal plane were measured using PIV. To extract the streaming component of the velocity field, the phase-locked ensemble average method was employed, as

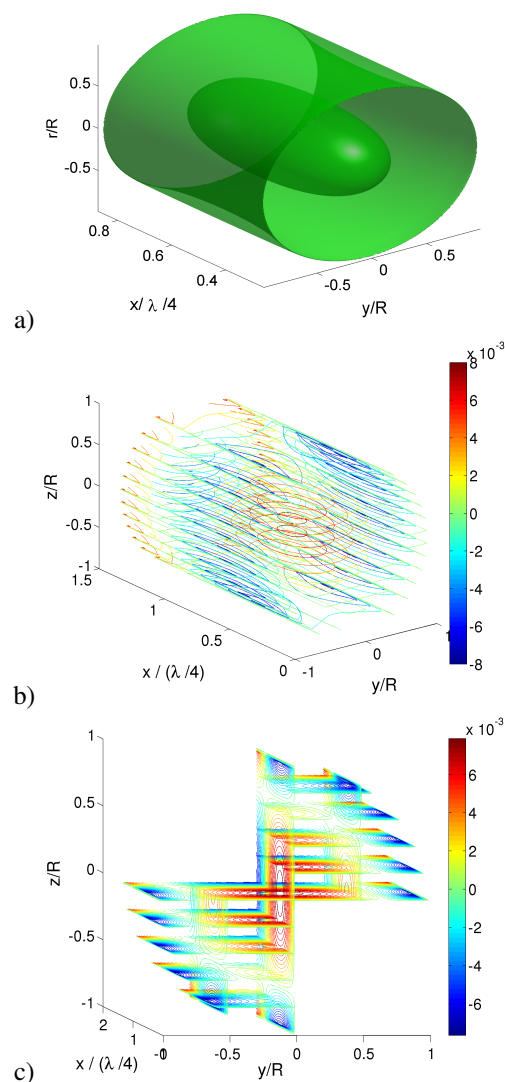


Figure 2: 3D schematic representation of the axial streaming velocity component in a cylindrical resonator.

described by Nabavi et al. [16]. The PIV system estimated the displacement of particles issued from the correlation of two images of the seeded field, the time step between the two images being exactly equal to the acoustic period, so that the acoustic component of the velocity naturally vanishes from this estimation of the velocity. At the phase corresponding to maximum acoustic velocity, 300 images, equally spaced in time by the acoustic period, were captured, yielding the calculated streaming velocity that is therefore an average over 299 values.

The system was driven at its third mode, corresponding to $L = 3\lambda/4$ i.e. to $f_{ac} = 245 \text{ Hz}$. The loudspeaker input voltage was set so that the acoustic velocity amplitude was equal to 3.4 m/s to limit non-linear propagation effects and thus higher harmonics generation in the guide. For $L = 3\lambda/4$, the length of a streaming cell, $\lambda/4$, is about 0.35 m . In order to obtain a sufficient spatial resolution, the studied streaming cell was divided into six equal intervals corresponding to the length of the camera field. The central streaming cell was scanned at 6 successive axial positions with an overlap of 0.5 cm . The size of the camera field was $7 \text{ cm} \times 7 \text{ cm}$, thus the spatial resolution of the PIV image is $\Delta x = \Delta y = 0.47 \text{ mm}$. Figure 4 shows an example of the measurement results of

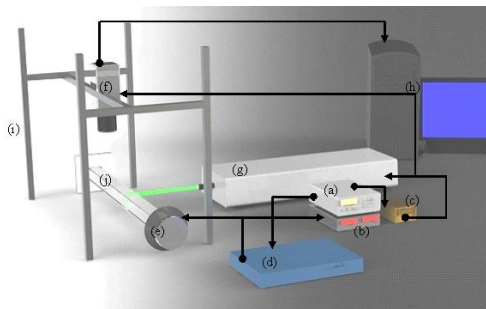


Figure 3: The experimental setup. (a) Function generator; (b) Power analyzer; (c) Synchronization unit; (d) Power amplifier; (e) Acoustic driver; (f) CCD camera; (g) Laser; (h) Computer with frame grabber; (i) Traversing mechanism; (j) Resonator tube.

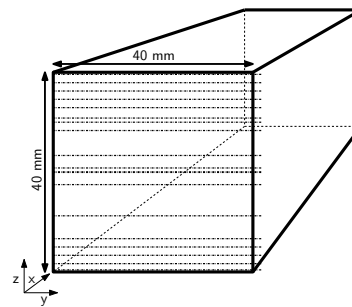


Figure 6: Representation of the 18 vertical position at which the velocity field was captured. x : axial direction, y : transverse direction, z : horizontal direction.

the axial component of the streaming velocity u_{2x} for the six camera positions, and Figure 5 shows the corresponding reconstructed streaming cell.

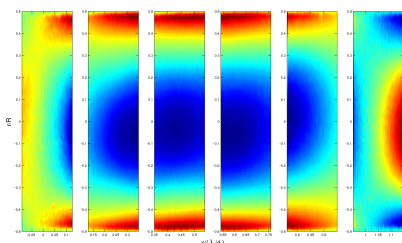


Figure 4: Example of results for u_{2x} measurements for the different camera fields. Here the Laser plane was set at $z/R = 0$, i.e. at the mid-height of the resonator.

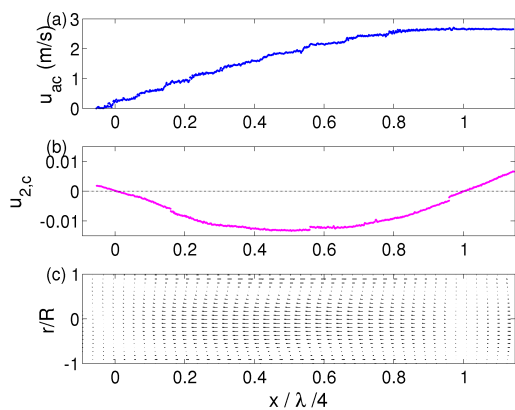


Figure 5: Typical results : (a) acoustic velocity and (b) u_{2c} . (c) Velocity vectors corresponding to the streaming field.

Measurements were performed at 18 vertical positions, as shown in Figure 6 so that 3D streaming cell structures could be reconstructed from the different planar streaming velocity fields. In order to resolve the velocity with better accuracy in the near wall region, a set of experiments was also performed near the wall of the channel. Twenty-five vertical fields were scanned at the location along the x -axis corresponding to the maximum streaming velocity. For these zoomed measurements, the size of the camera field was $6.5\text{mm} \times 5\text{mm}$ consequently the spatial resolution of the PIV image was $\Delta x = \Delta y = 0.04\text{mm}$.

4 Results

Figure 7 shows an isovelocity representation of the measured streaming structure. The corresponding theoretical prediction is shown in Figure 2.a. This first qualitative comparison suggests that overall, outer streaming vortices are not greatly influenced by the geometry of the resonator section, as the theoretical and experimental outer vortices have the same shape and dimensions along the axial and transverse dimensions. However, streaming in the near wall region seems to differ significantly in a square resonator compared to the case of a cylindrical guide. In order highlight this trend, axial and transverse profiles of the axial component of the streaming velocity were obtained. Figure 8 shows a comparison be-

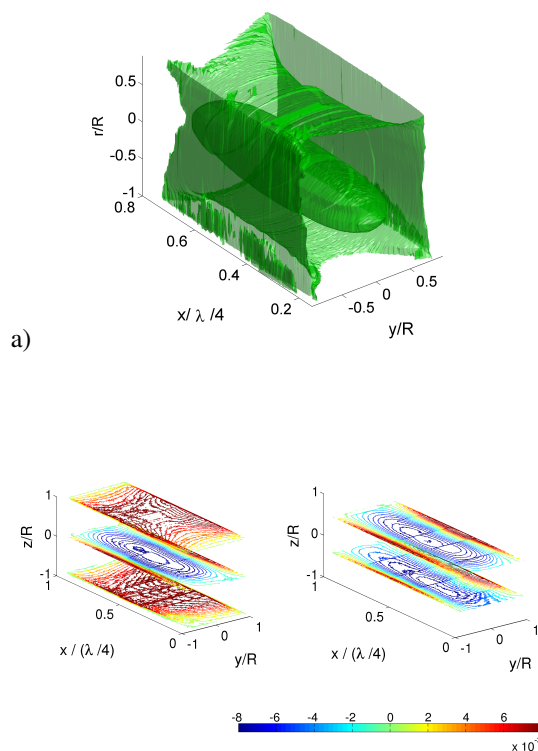


Figure 7: a) Isosurfaces showing points of streaming velocity magnitudes equal to 0.006m/s over a measured streaming cell. b) 3D reconstruction of a streaming cell measured by PIV

tween measured centerline axial streaming velocity and the corresponding theoretical prediction, u_{2c} , as calculated from

[8]. Here and in the following, the streaming velocity is presented in an a-dimensional form, being divided by the maximum Rayleigh axial streaming velocity given by $\frac{3A^2}{8c}$, where A is the amplitude of the acoustic velocity at the acoustic velocity antinode. As shown by this Figure, the measured centerline streaming velocity is in excellent agreement with the theoretical prediction for a cylindrical guide.

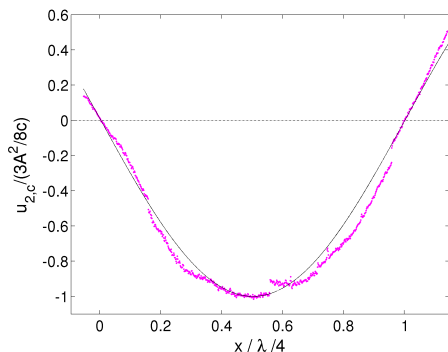


Figure 8: Calculated (solid line) axial component of the centerline streaming velocity along the waveguide axis compared to the measured one (pink points).

Data in the near wall region are shown in Figure 9 that corresponds to similar comparison for $z = 0.945R$. The measured and calculated axial profiles were in good agreement.

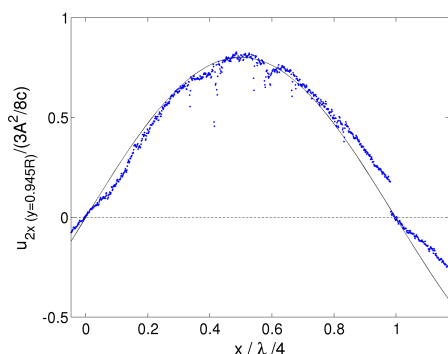


Figure 9: Axial profile of $u_{2,x}$ near the resonator wall, at $z = 0.945R$. Solid line: calculation for a cylindrical waveguide. Blue dots: measured in a square-section resonator.

Figure 10 shows both y and z profiles for $u_{2,x}$ measured and calculated using [8]. The z profile was reconstructed from the different velocity fields scanned as shown by Figure 6. Here the profiles are given for the x position corresponding to the centre of the streaming cell, i.e. $x = \lambda/8$. Considering the difficulty of reconstructing a z -profile from different horizontal velocity fields, the results are very satisfactory. Here again, the experimental and theoretical results are in good agreement. For this position, the measured z and y transverse profiles comparable, symmetric, and in agreement with the theoretical 2D predictions. Note that, as discussed in Section 2, streaming in a square-section waveguide appears to be close to streaming in cylindrical waveguide, $u_{2,x}$ going from $\frac{3A^2}{8c}$ in the centerline to $-\frac{3A^2}{8c}$ in the near wall region for the outer cell whereas streaming between two infinite plates goes from $\frac{3A^2}{16c}$ to $-\frac{3A^2}{8c}$ [9]. It is necessary to focus on the near wall region to be able to characterize the 3D feature of streaming in a square section resonator. Figure 11 shows transverse

profiles for near wall region: at $z = 0.945R$ and at $z = 0.85R$. This figure reveals that very close to the wall, from about 15 viscous penetration depth from the wall, the streaming structure starts to deviate from the theoretical expectation for a cylindrical guide. Indeed, for $z = 0.85R$ both theoretical and experimental streaming feature a characteristic parabolic profile outside the near wall region whereas for $z = 0.945R$ the measured streaming departs from this shape. Note that this last measurements suffers from a slight misalignment between the laser plane and the horizontal plane so that the measured streaming is not symmetric with respect to the y axis. The accuracy of the results for $0 < y < 1$ is doubtful. Nevertheless Figure 11a shows that the transverse position of the limit between the outer and the inner vortices differs significantly in the case of a cylindrical waveguide (change of cell at about $y = 0.7R$) and in the case of a square-section resonator (change of cell at about $y = 0.9R$). This is even more clear when considering measurement results in the zoomed configuration (size of the camera field equal to $6\text{mm} \times 5.5\text{mm}$) shown in figure 12 which shows a comparison between near wall (from 0 to $35\delta_v$) measured and calculated y profiles of $u_{2,x}$ for planes at different z locations : from $z = 0.98R$ or $1 - z = 2.3\delta_v$ (figure 12.a) to $z = 0$ (figure 12.c). In the cylindrical case, because we slice toroidal vortices according to z , the position of the limit between inner and outer vortices depends on the considered z plane. On the contrary and in agreement with figure 7.a, the position of the limit between inner and outer cells does not change with the considered z -slice for a square-section configuration so that the flow structure in the near wall region is coherent with the guide geometry.

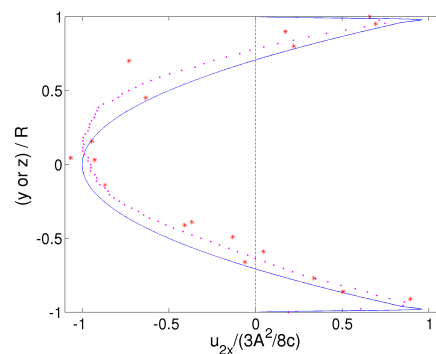


Figure 10: Calculated (solid line) $u_{2,x}$ along the transverse direction compared to measured one. (.) : measured along the y -axis and (*) : reconstructed profile along the z -axis.

5 Conclusion

The study of streaming velocity fields in a square-section waveguide, based on PIV measurements and comparisons with calculations in an ideal cylindrical case, shows that streaming in a square-section waveguide has many similarities to streaming in cylindrical waveguide, being therefore quite different from the case of two infinite rectangular plates. Streaming in non-cylindrical resonators is significantly different from in cylindrical resonators in the very near wall region only. Although this region corresponds to those of streaming driving force, these differences do not seem to have an influence on the overall shape of the streaming cells. However, regions

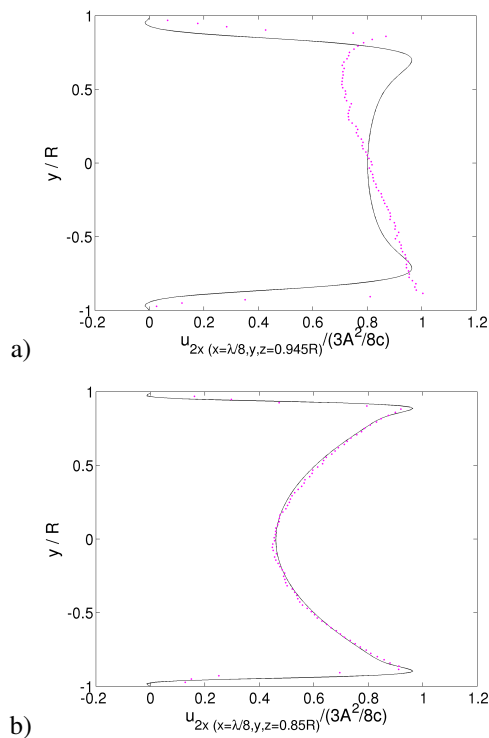


Figure 11: (a) Transverse profile of u_{2x} at $z = 0.945R$ at x position corresponding to the maximum streaming velocity ($\lambda/8$), (b) Transverse profile at $z = 0.85R$ at x position corresponding to the maximum of streaming velocity.

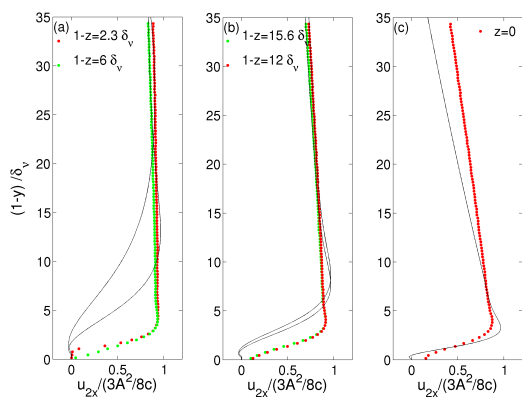


Figure 12: Transverse profile of $u_{2x}(x = \lambda/8)$ for different z positions. Solid line: calculation. Dots: experimental data. The y -axis is adimensionized by δ_v .

where fluid to solid heat transfer occurs scale as inner vortices width. Therefore, because in these regions the actual streaming velocities noticeably differ from the ones obtained from available theoretical models, the actual heat transfer effects associated to streaming mass flow can be expected to deviate from theoretical one when a non-ideal shape is used.

Acknowledgments

Hélène Bailliet thanks the Region Poitou Charente for financial help. Ida Reyt acknowledges financial support from Ecole Doctorale SIMMEA. This study was founded in part by The Natural Sciences and Engineering Research Council of Canada.

References

- [1] L. Rayleigh, "The theory of sound", Dover, New York, 2nd ed. (2), (1945)
- [2] I. Paek, L. Mongeau, J. Braun "Performance characterization of a small-capacity thermoacoustic cooler for air-conditioning applications", *J. Mech. Sc. and Tech.*, 24(9), 1781-1791, (2010)
- [3] L. Rayleigh, "On the circulation of air observed in Kundt's tubes, and on some allied acoustical problems", *Philos. Trans. R. Soc. London* 175, 1-21, (1884)
- [4] W.L. Nyborg, "Acoustic streaming", in *Physical Acoustics*, edited by W. P. Mason (Academic, New York, 1965), 2B(11), 290-295, (1965)
- [5] P.J. Westervelt, "The theory of steady rotational flow generated by sound field" *J. Acoust. Soc. Am.*, 25, 60-67, (1953)
- [6] Q. Qi, R. Johnson, J. Harris, "Boundary layer attenuation and acoustic streaming accompanying plane-wave propagation in a tube", *J. Acoust. Soc. Am.*, 97(3), 1499-1509, (1995)
- [7] N. Rott, "The influence of heat conduction on acoustic streaming", *J. of Applied Mathematics and Physics (ZAMP)*, 25, 417-421, (1974)
- [8] H. Bailliet, V. Gusev, R. Raspet and R. A. Hiller, "Acoustic streaming in closed thermoacoustic devices", *J. Acoust. Soc. Am.*, 110, 1808-1821, (2001)
- [9] M. Hamilton, Y. Ilinski, E. Zabolotskaya, "Thermal effects on acoustic streaming in standing waves", *J. Acoust. Soc. Am.*, 114, 3092-3101, (2003)
- [10] L. Menguy, J. Gilbert, "Non-linear acoustic streaming accompanying a plane stationary wave in a guide" *Acustica*, 86, 249-259, (2000)
- [11] J.P. Sharpe, C.A. Greated, C. Gray, D.M. Campbell, "The measurements of acoustic streaming using particle image velocimetry", *Acustica*, 68, 168-172, (1989)
- [12] D.M. Campbell, J. Cosgrove, C.A. Greated, S. Jack, D. Rockliff, "Review of LDA and PIV applied to the measurement of sound and acoustic streaming", *Optics and Laser Technology*, 32, 629-639, (2000)
- [13] M. Thompson, A. Atchley, "Simultaneous measurement of acoustic and streaming velocities in a standing wave using Laser Doppler Anemometry", *J. Acoust. Soc. Am.*, 117, 1828-1838, (2005)
- [14] M. Thompson, A. Atchley, M. Maccarone, "Influences of a temperature gradient and fluid inertia on acoustic streaming in a standing wave", *J. Acoust. Soc. Am.*, 117, 1839-1849, (2005)
- [15] S. Moreau, H. Bailliet, J.C. Valière, "Measurement of inner and outer streaming vortices in a standing wave guide using Laser Doppler Velocimetry (LDV)", *J. Acoust. Soc. Am.*, 123(2), (2007)
- [16] M. Nabavi, M. H. K. S. Dargahi, "Experimental investigation of the formation of acoustic streaming in a rectangular enclosure using a synchronized PIV technique", *Meas. Sci. Technol.*, 19(6), (2008)
- [17] G. Swift, "Thermoacoustic engines", *J. Acoust. Soc. Am.*, 88, 1145-1180, (1988)
- [18] W. Arnott, H. Bass, R. Raspet, "General formulation of thermoacoustics for stacks having arbitrarily shaped pore cross sections" *J. Acoust. Soc. Am.*, 90(6), 3228-3237, (1991)